AIAA JOURNAL
Vol. 39, No. 8, August 2001

Monotone Residual Distribution Schemes for the Ideal Magnetohydrodynamic Equations on Unstructured Grids

Árpád Csík* and Herman Deconinck†
von Kármán Institute for Fluid Dynamics, B-1640 Sint-Genesius-Rode, Belgium
and
Stefaan Poedts‡
Katholieke Universiteit Leuven, B-3001 Leuven, Belgium

Multidimensional upwind residual distribution schemes are applied to the eight-wave equations of ideal magnetohydrodynamics. These schemes extend the high-resolution upwind finite volume methodology to a truly multidimensional finite element context on unstructured grids. Both first- and second-order linear and second-order nonlinear monotonicity preserving schemes are discussed. An approximate conservative linearization technique is derived for general hyperbolic systems together with a conservative correction technique, which guarantees the full conservation of the convective fluxes. The solenoidal condition of the magnetic field is enforced by Powell's source term approach. Both implicit and explicit time-integration strategies have been implemented. The spatial accuracy and the shock-capturing properties of the schemes in the steady state are investigated numerically. Computational results are presented for a bow shock over a cylinder and for a supermagnetosonic flow in a channel.

Introduction

THE magnetohydrodynamics (MHD) equations describe the behavior of conducting fluids under the presence of magnetic fields. They couple the equations of fluid dynamics with Maxwell's equations of electrodynamics. Many important and interesting phenomena both in laboratory[1] and in astrophysical[2,3] plasmas (ionized gases) can be successfully described by this macroscopic MHD model.

The full MHD equations are a complicated set of nonlinear partial differential equations, taking into account the combined effects of multispecies transport, relativistic processes, and dissipative phenomena such as heat conduction, viscosity, and resistivity. These will be neglected in the present paper because our interest exclusively goes to basic discontinuity capturing algorithms for Newtonian MHD simulations. The resulting simplified model is described by the single fluid compressible ideal MHD equations.

The idea of the residual distribution (fluctuation splitting) method as a multidimensional upwind spatial discretization technique for the Euler equations of gasdynamics is originated by Roe[4] and was further developed by the authors of Refs. 5–9. The multidimensional upwind schemes for scalar advection were extended to noncommuting hyperbolic systems by van der Weide et al.[10,11] by introducing positive coefficient matrix distribution schemes. Schemes constructed in this framework are designed to produce monotone solutions across steep gradients by generalizing total-variation-diminishing principles and Godunov schemes to unstructured grids composed of linear finite elements. The notion of positivity as a monotonicity concept has been used also in a pure finite volume context, where it is also known as local-extremum-diminishing (LED) property.[12]

In this paper we develop upwind multidimensional numerical schemes for the ideal MHD equations based on these latest developments for hydrodynamics. The fluctuation splitting method requires regular Jacobian matrices per cell. Because the original form of the MHD equations leads to singular Jacobian matrices, we solve the regularized eight-wave Galilean invariant ideal MHD equations[13] as proposed by Powell et al.[14,15] In this approach the singularity is removed by adding a source term proportional to $\nabla \cdot \boldsymbol{B}$ to the conservative form, hence introducing the so-called divergence wave. Consequently, the resulting equations are no longer in strict conservation form, which can occasionally lead to inconsistent jumps accross very strong shocks, as has been demonstrated in recent literature.[16] Nevertheless, for a certain range of applications good results have been demonstrated.[15,17] The weak enforcement of the so-called divergence-free condition also stabilizes the numerical scheme against the instabilities related to the numerically nonvanishing divergence of the magnetic field.

In the finite volume context the solenoidal condition is often treated in a fully conservative way by a staggered grid approach. However, this method strongly relies on the geometry of the mesh and cannot be applied in a finite element context on unstructured grids.[16]

The structure of this paper is as follows. In the second section we give a brief introduction into the MHD equations. In the third section we summarize the basic principles of the fluctuation splitting method for systems of conservation laws, in particular for the ideal MHD equations. The time-integration strategies are described in the fourth section. In the fifth section we present an upwind multidimensional MHD code. In the sixth section we demonstrate its advanced properties through numerical test results. Some concluding remarks are given in the last section.

Governing Equations of Ideal MHD

The unsteady hyperbolic system of ideal single-fluid nonrelativistic MHD equations in conservative form is given by

$$\frac{\partial U}{\partial t} + \nabla \cdot \boldsymbol{F} = 0 \tag{1}$$

where the state vector U in conservative variables and the conservative flux vector $\boldsymbol{F}$ containing the isotropic pressure tensor are

$$U = (\rho, \rho u, \rho v, \rho w, B_x, B_y, B_z, E)^T \tag{2}$$

Presented as Paper 99-3325 at the AIAA 14th Computational Fluid Dymanics Conference, Norfolk, VA, 28 June–1 July 1999; received 14 July 2000; revision received 22 February 2001; accepted for publication 8 March 2001.

*Ph.D. Candidate, Department of Aeronautics and Aerospace, Chaussée de Waterloo 72, and Center for Plasma Astrophysics, Department of Mathematics, Katholieke Universiteit Leuven, Celestijnenlaan 200B, B-3001 Leuven, Belgium; arpi@vki.ac.be.

†Professor and Head, Department of Aeronautics and Aerospace, Chaussée de Waterloo 75; deconinck@vki.ac.be. Member AIAA.

‡Professor and Research Associate of the F.W.O.-Vlaanderen, Center for Plasma Astrophysics, Department of Mathematics, Celestijnenlaan 200B; stefaan.Poedts@wis.kuleuven.ac.be.

$$\boldsymbol{F} = \begin{pmatrix} \rho \boldsymbol{v} \\ \rho \boldsymbol{v}\boldsymbol{v} + \hat{I}(p + \boldsymbol{B}\cdot\boldsymbol{B}/2) - \boldsymbol{B}\boldsymbol{B} \\ \boldsymbol{v}\boldsymbol{B} - \boldsymbol{B}\boldsymbol{v} \\ (E + p + \boldsymbol{B}\cdot\boldsymbol{B}/2)\boldsymbol{v} - \boldsymbol{B}(\boldsymbol{v}\cdot\boldsymbol{B}) \end{pmatrix} \tag{3}$$

Here superscript T stands for the transposed vector; $\hat{I}$ represents the 3×3 identity matrix; ρ is the density; u, v, and w are the x, y, and z components of the velocity $\boldsymbol{v}$; $\boldsymbol{B}$ is the magnetic field; p is the thermal pressure; and E is the total energy density defined by

$$E = p/(\gamma - 1) + \tfrac{1}{2}\rho \boldsymbol{v}\cdot\boldsymbol{v} + \tfrac{1}{2}\boldsymbol{B}\cdot\boldsymbol{B} \tag{4}$$

where γ is the ratio of specific heats. In this paper we use units such that the magnetic permeability μ_0 is unity; therefore, it does not show up in the equations. As a consequence, the physical magnetic pressure (based on the unscaled magnetic vector $\hat{\boldsymbol{B}}$)[2,18] in SI units defined by $p^B = \hat{\boldsymbol{B}}\cdot\hat{\boldsymbol{B}}/2\mu_0$ takes the form: $p^B = \boldsymbol{B}\cdot\boldsymbol{B}/2$. Equation (1) describes the conservation of mass, momentum, magnetic flux, and energy and is to be supplemented by the divergence-free condition of the magnetic field:

$$\nabla\cdot\boldsymbol{B} = 0 \tag{5}$$

The latter constraint expresses the observational fact that magnetic monopoles do not exist. In an analytical treatment Eq. (5) is merely an initial constraint because the evolution equation of the magnetic field guaranties its validity at all times when it is initially satisfied. However, in a numerical approach, because of the discretization and the round-off errors, the divergence of the magnetic field may deviate from zero, which has a destabilizing effect on a numerical algorithm. A popular way to stabilize the MHD equations against this numerical instability is to add a source term[14] (denoted as Powell's source term in the following) to the right-hand side of Eq. (1), leading to the unique nonconservative Galilean invariant symmetrizable form of the ideal MHD equations[13]:

$$\frac{\partial U}{\partial t} + \nabla\cdot\boldsymbol{F} = S \tag{6}$$

Here S is defined by

$$S = -s\nabla\cdot\boldsymbol{B} \tag{7}$$

with $s = [0, B_x, B_y, B_z, u, v, w, \boldsymbol{v}\cdot\boldsymbol{B}]^T$. Equation (6) is equivalent to the conservation law (1) at the partial differential equation level, but the discretization of the modified system has much better numerical stability properties.

Consider now the quasilinear form of Eq. (6) in terms of the conservative variables, in two space dimensions:

$$\frac{\partial U}{\partial t} + A_U^{'}\frac{\partial U}{\partial x} + B_U^{'}\frac{\partial U}{\partial y} = S \tag{8}$$

Here $A_U^{'} = \partial F_x/\partial U$ and $B_U^{'} = \partial F_y/\partial U$ are the Jacobian matrices. Because the source term S is proportional to $\nabla\cdot\boldsymbol{B}$, we can reformulate Eq. (8) by introducing matrix notations for the description of S:

$$\frac{\partial U}{\partial t} + A_U^{'}\frac{\partial U}{\partial x} + B_U^{'}\frac{\partial U}{\partial y} = -\left(S_x\frac{\partial U}{\partial x} + S_y\frac{\partial U}{\partial y}\right) \tag{9}$$

where the fifth and sixth column of the source matrices S_x and S_y equal vector s, while all other elements vanish. This formulation allows us to rewrite Eq. (8) as

$$\frac{\partial U}{\partial t} + A_U\frac{\partial U}{\partial x} + B_U\frac{\partial U}{\partial y} = 0 \tag{10}$$

where $A_U = A_U^{'} + S_x$ and $B_U = B_U^{'} + S_y$.

Consider the set of primitive variables $P = [\rho, u, v, w, B_x, B_y, B_z, p]^T$ connected to the conservative variables U by the similarity transformation $\partial P = (\partial P/\partial U)\partial U$. The regularized hyperbolic system (10) then transforms into

$$\frac{\partial P}{\partial t} + A_P\frac{\partial P}{\partial x} + B_P\frac{\partial P}{\partial y} = 0 \tag{11}$$

where $A_P = (\partial P/\partial U)A_U(\partial U/\partial P)$ and $B_P = (\partial P/\partial U)B_U(\partial U/\partial P)$ are the Jacobian matrices of the regularized system in primitive variables. For example, matrix A_P reads

$$A_P = \begin{pmatrix} u & \rho & 0 & 0 & 0 & 0 & 0 & 0 \\ 0 & u & 0 & 0 & 0 & B_y/\rho & B_z/\rho & 1/\rho \\ 0 & 0 & u & 0 & 0 & -B_x/\rho & 0 & 0 \\ 0 & 0 & 0 & u & 0 & 0 & -B_x/\rho & 0 \\ 0 & 0 & 0 & 0 & u & 0 & 0 & 0 \\ 0 & B_y & -B_x & 0 & 0 & u & 0 & 0 \\ 0 & B_z & 0 & -B_x & 0 & 0 & u & 0 \\ 0 & \gamma p & 0 & 0 & 0 & 0 & 0 & u \end{pmatrix}$$

whereas for the original system (1) this matrix is singular and its fifth row contains only zeros.

Fluctuation Splitting Spatial Discretization

We solve the eight-wave MHD equations (6) with the Powell source term on an arbitrary triangulation of the spatial domain Ω, based on the residual distribution method. The area of an elementary triangle is labeled by S_T, and its geometry is given in Fig. 1. Just as in linear finite element methods, the solution is approximated by a continuous function, varying linearly over each triangle:

$$U(x, y, t) = \sum_i U_i(t)N_i(x, y) \tag{12}$$

where $U_i(t)$ is the time-dependent value $U(x_i, y_i, t)$ at node i and the piecewise linear shape function $N_i(x, y)$ equal to unity at node i and vanishing outside the support of all triangles meeting at node i.

Assume that Eq. (10) has been linearized over a triangular cell T, such that it is equivalent to Eq. (6) at the discrete level (see section on Conservative Linearization). Integration of Eq. (10) then leads to the definition of the fluctuation Φ^T in triangle T:

$$\Phi^T = -\iint_T \frac{\partial U}{\partial t}\,\mathrm{d}\Omega = \iint_T \left(A_U\frac{\partial U}{\partial x} + B_U\frac{\partial U}{\partial y}\right)\mathrm{d}\Omega \tag{13}$$

where A_U and B_U are constant matrices for each triangle. By using Gauss's theorem, the fluctuation Φ^T can also be written as a contour integral along the boundary Γ of triangle T:

$$\Phi^T = (A_U\boldsymbol{i} + B_U\boldsymbol{j})\iint_T \nabla U\,\mathrm{d}\Omega = \oint_\Gamma (A_U n_{x,\mathrm{out}} + B_U n_{y,\mathrm{out}})U\,\mathrm{d}\Gamma \tag{14}$$

where $\boldsymbol{i}$ and $\boldsymbol{j}$ are the unit vectors in the x and y directions, respectively, and $n_{x,\mathrm{out}}$ and $n_{y,\mathrm{out}}$ are the x and y components of the

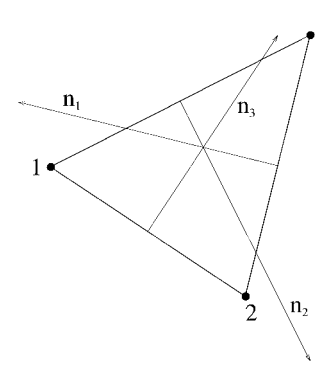

Fig. 1 General triangle with inward scaled normals n_1, n_2, and n_3.

outward showing unit normals. Because the variation of the conservative state vector U is piecewise linear, ∇U is constant in triangle T, and it can be expressed in terms of the inward pointing face normals $\boldsymbol{n}_i = n_{x,i}\boldsymbol{i} + n_{y,i}\boldsymbol{j}$, scaled with the length of the edge (see Fig. 1), and the solution vector U_i at node i:

$$\nabla U = \frac{1}{2S_T}\sum_{i=1}^{3} U_i \boldsymbol{n}_i \tag{15}$$

Combining Eqs. (14) and (15), the cell residual Φ^T is written as

$$\Phi^T = \sum_{i=1}^{3} K_i U_i \tag{16}$$

where matrix K_i is defined by the following linear combination of the Jacobians:

$$K_i = \tfrac{1}{2}(A_U n_{x,i} + B_U n_{y,i}) \tag{17}$$

Although the system of ideal MHD equations is hyperbolic, it is not strictly hyperbolic in the sense that some of the eigenvalues may be equal for certain values of U, which are called *umbilic points* in the phase space. However, K_i has real eigenvalues and a complete set of left and right real eigenvectors. Unfortunately, these classical eigenvectors are degenerate at the umbilic points. The degeneracies can be removed by applying a proper scaling.[14,19–21] Diagonalization of matrix K_i yields

$$K_i = \tfrac{1}{2} R_i \Lambda_i L_i \tag{18}$$

where the columns of R_i are the scaled right eigenvectors, the rows of L_i are the scaled left eigenvectors, and Λ_i is the diagonal matrix of the eigenvalues proportional to $|\boldsymbol{n}_i|$. Omitting index i for convenience, the eigenvalues of matrix K are

$$\Lambda_1 = (\boldsymbol{v}\cdot\boldsymbol{n} - c_f|\boldsymbol{n}|)/2, \qquad \Lambda_2 = (\boldsymbol{v}\cdot\boldsymbol{n} - c_A|\boldsymbol{n}|)/2$$

$$\Lambda_3 = (\boldsymbol{v}\cdot\boldsymbol{n} - c_s|\boldsymbol{n}|)/2, \qquad \Lambda_4 = \boldsymbol{v}\cdot\boldsymbol{n}/2$$

$$\Lambda_5 = \boldsymbol{v}\cdot\boldsymbol{n}/2, \qquad \Lambda_6 = (\boldsymbol{v}\cdot\boldsymbol{n} + c_s|\boldsymbol{n}|)/2$$

$$\Lambda_7 = (\boldsymbol{v}\cdot\boldsymbol{n} + c_A|\boldsymbol{n}|)/2, \qquad \Lambda_8 = (\boldsymbol{v}\cdot\boldsymbol{n} + c_f|\boldsymbol{n}|)/2$$

The fast and slow magnetosonic speeds c_f and c_s and the Alfvén speed c_A are given by the following expressions:

$$c_{f,s}^2 = \frac{1}{2}\left[a^2 \pm \sqrt{a^4 - \frac{4\gamma p(\boldsymbol{B}\cdot\boldsymbol{n})^2}{(\rho|\boldsymbol{n}|)^2}}\right] \tag{19}$$

$$c_A = \frac{\boldsymbol{B}\cdot\boldsymbol{n}}{\sqrt{\rho}\,|\boldsymbol{n}|} \tag{20}$$

with

$$a^2 = (\gamma p + \boldsymbol{B}\cdot\boldsymbol{B})/\rho \tag{21}$$

Matrices K_i^+ and K_i^- are the so-called generalized upwind parameters, defined by

$$K_i^+ = \tfrac{1}{2} R_i \Lambda_i^+ L_i \tag{22}$$

$$K_i^- = \tfrac{1}{2} R_i \Lambda_i^- L_i \tag{23}$$

where Λ_i^+ and Λ_i^- contain the positive and negative eigenvalues, respectively: $\Lambda_i^\pm = (\Lambda_i \pm |\Lambda_i|)/2$.

In the fluctuation splitting approach the cell residual Φ^T is computed, and its fractions are distributed to the nodes of triangle T. The contributions from all cells to a given node are assembled, giving the nodal update. This treatment leads to a very compact stencil involving only the nearest neighbors in the triangulation, which is useful for efficient parallelization and implicit time-integration strategies. The semidiscretized form of Eq. (10) at point i, with the most simple treatment of the time derivative (corresponding to lumping the Galerkin mass matrix in finite elements), is given by

$$\frac{\mathrm{d}U_i}{\mathrm{d}t} = -\frac{1}{S_i}\sum_{T,\,i\in T}\beta_i^T\Phi^T = -\frac{1}{S_i}\sum_{T,\,i\in T}\Phi_i^T \tag{24}$$

Here S_i is the area of the median dual cell around node i equal to $\frac{1}{3}$ of the area of all triangles sharing node i, β_i^T is the distribution matrix to node i in triangle T, and the distribution function $\Phi_i^T = \beta_i^T\Phi^T$ is the fraction of the residual in triangle T sent to node i. To keep the consistency of the scheme, it is required that

$$\sum_{i=1}^{3}\beta_i^T = \hat{I} \tag{25}$$

where the index i goes over the local number of nodes in triangle T.

The properties of the different schemes in the fluctuation splitting context are determined by the way β_i^T is defined. A monotonic solution satisfying the LED property can be obtained by demanding positivity of the coefficients of the unknowns in the update equation. The solution of a positive scheme is free of spurious oscillations close to discontinuities. A scheme is called linearity preserving if it reproduces the exact solution of the problem in the steady state, when this solution is a linear function of the spatial variables. In smooth flows linearity-preserving schemes in practice will lead to second-order accuracy at the steady state, although in a strict sense only order of 1.5 is obtained on arbitrary meshes according to a Petrov–Galerkin finite element analysis.[22] Godunov's theorem for multidimensional schemes states that only nonlinear schemes can be positive and linearity preserving at the same time. A more detailed description of these properties is given by van der Weide[10,11] and Deconinck et al.[23] In the following paragraphs we present two first-order linear monotone, a second-order linear nonmonotone, and a second-order nonlinear monotone scheme.

First-Order Linear System N Scheme

The linear system N scheme (narrow) is positive (T. J. Barth, "Some Working Notes on Energy Analysis of the N Scheme," private communication, 1996); therefore, it is monotonicity preserving at extremas and at most first-order accurate according to Godunov's theorem. The distribution function $\beta_i^T\Phi^T$ is given by

$$\beta_i^T\Phi^T = K_i^+\left(\sum_{j=1}^{3}K_j^-\right)^{-1}\sum_{j=1}^{3}K_j^-(U_i - U_j) \tag{26}$$

The residual Φ_i^N sent to node i in triangle T by the N scheme reduces to

$$\Phi_i^N = \beta_i^T\Phi^T = K_i^+(U_i - U_{\mathrm{in}}) \tag{27}$$

where the state U_{in} is defined by

$$U_{\mathrm{in}} = \left(\sum_{j=1}^{3}K_j^-\right)^{-1}\sum_{k=1}^{3}K_k^-U_k \tag{28}$$

It is shown by Abgrall[24] that for a linearized symmetrizable system the N and low diffusion A (LDA) schemes are always well defined, even in the case when

$$\sum_{j=1}^{3}K_j^-$$

has a vanishing eigenvalue (e.g., stagnant flow).

First-Order Linear Finite Volume Scheme

The standard first-order upwind finite volume (FV) scheme, which is positive and therefore LED, can be reformulated on the median dual mesh in terms of the fluctuation splitting method. The fluctuation Φ^T in triangle T can be computed as

$$\Phi^T = K_{12}(U_2 - U_1) + K_{23}(U_3 - U_2) + K_{31}(U_1 - U_3) \tag{29}$$

where the matrices K_{ij} are now defined with combinations of the median dual cell normals $\boldsymbol{n}_{ij} = (\boldsymbol{n}_j - \boldsymbol{n}_i)/6$ by the following equation:

$$K_{ij} = A_U n_{x,ij} + B_U n_{y,ij} \tag{30}$$

The definition of the distribution function Φ^{FV} corresponding to the positive first-order FV scheme is then

$$\Phi_i^{FV} = K_{ij}^-(U_j - U_i) + K_{ki}^+(U_i - U_k) \tag{31}$$

Second-Order Linear System LDA Scheme

The linear system LDA scheme satisfies the linearity preservation property, and hence it is not positive. The distribution matrix is given by

$$\beta_i^T = K_i^+ \left(\sum_{j=1}^{3} K_j^+ \right)^{-1} \tag{32}$$

The distribution function Φ^{LDA} for the LDA scheme is

$$\Phi_i^{LDA} = \beta_i^T \Phi^T = K_i^+ \left(\sum_{j=1}^{3} K_j^+ \right)^{-1} \Phi^T \tag{33}$$

Second-Order Nonlinear Blended Scheme

By applying a nonlinear blending on the distribution coefficients of two linear schemes just described, it is possible to construct a nonlinear scheme that presents a monotone shock-capturing property and second-order accuracy away of shocks in practical simulations. The positive N scheme captures the discontinuities without spurious spatial oscillations, but its accuracy is only first order. The linearity-preserving LDA scheme is second-order accurate in smooth domains, but it is not suitable for flows containing discontinuities. To combine the advantages of both of these schemes, we define the residual distributed to node i in a triangle as

$$\Phi_i^B = (\hat{I} - \Theta)\Phi_i^{LDA} + \Theta\Phi_i^N \tag{34}$$

where the nonlinear blending coefficient Θ is a diagonal matrix defined as

$$\Theta_{lm} = \frac{\left|\Phi_m^T\right|}{\sum_{j=1}^{3} \left|\Phi_{j,m}^N\right|}\delta_{lm} \qquad \text{if} \qquad \sum_{j=1}^{3} \left|\Phi_{j,m}^N\right| > \epsilon$$

$$\Theta_{lm} = 0 \qquad \text{if} \qquad \sum_{j=1}^{3} \left|\Phi_{j,m}^N\right| \le \epsilon \tag{35}$$

Here index j goes through the local numbering of the nodes in triangle T, and the m index refers to the mth component of state vector U. ϵ represents the machine zero, which equals 10^{-14} in practical simulations. Definition (35) shows that the blending is applied in a scalar way, meaning that for each of the equations we define a blending coefficient $\theta_m = \Theta_{m,m}$. Equations (35) imply that the diagonal elements θ_m of the blending matrix Θ satisfy the relation $0 \le \theta_m \le 1$ because

$$\Phi_m^T = \sum_{j=1}^{3} \Phi_{j,m}^N$$

For scalar equations the exact positivity of the blended scheme can be proven for an appropriate definition of the blending coefficient θ. Unfortunately, this does not generalize to the system case, although in practice also for systems it gives monotone solutions accross discontinuities. The reason is that according to numerical experiments (and theoretical estimations) at the steady state $|\Phi_m^T| = \mathcal{O}(|\Phi_{j,m}^N|)$ near discontinuities because the cell residual is far from equilibrium, whereas $|\Phi_m^T| \approx h^3$ in smooth flows (h is an average mesh size). Hence $\theta_m \approx 1$ near discontinuities, and $\theta_m \approx 0$ in smooth flows.

Consequently, the contribution of the monotone first-order N scheme in the blended residual enforces monotonicity across steep gradients, and in smooth flows the blended scheme is very close to the second-order LDA scheme. The definition of the blending coefficient (35) implies the linearity preservation property: $\Phi_i^B \to 0$ if $\Phi^T \to 0$.

A more sophisticated blended scheme based on entropy considerations was recently developed by Abgrall.[24]

Conservative Linearization

For the monotone fluctuation splitting schemes described in the preceding subsections (FV, N, and B schemes), it is necessary to have a quasilinear form (10) of the conservation law with the source term (6), whereby constant Jacobian matrices are assumed in each cell. However, in order to capture the discontinuities with the correct jump relations, the convective fluxes have to be discretized in a conservative way. The solution to this problem is known as the conservative linearization.

In the context of Euler flows, such a linearization is given by the Roe-linearization obtained by assuming linear variation of the Roe parameter vector over the triangle.[5] A generalization to the MHD equations turns out to be much more complex. Let us integrate the advection and the source terms in Eq. (6) and the corresponding terms in the quasilinear form (10) over a control volume. Exact integration of the fluxes and the source term requires the satisfaction of the following constraint:

$$\oint_{\partial T} \boldsymbol{F} \cdot \boldsymbol{n}\, \mathrm{d}l - \iint_T S\, \mathrm{d}\Omega = \iint_T \left(\frac{\partial F_x}{\partial x} + \frac{\partial F_y}{\partial y} - S \right) \mathrm{d}\Omega$$

$$= (\widehat{A_Z}\boldsymbol{i} + \widehat{B_Z}\boldsymbol{j}) \iint_T \nabla Z\, \mathrm{d}\Omega \tag{36}$$

where Z is a set of independent variables, not necessarily the conservative ones, $\widehat{A_Z}$ and $\widehat{B_Z}$ are the constant Jacobian matrices taken at the averaged state $\bar{Z}$, and $\boldsymbol{i}$ and $\boldsymbol{j}$ are the unit vectors in the x and y directions, respectively. Assuming linear variation of Z over triangle T and taking into account the form of the source term, Eq. (36) can be written in the following, more restrictive form:

$$\iint_T \left(\frac{\partial F_x}{\partial Z} + S_x \frac{\partial U}{\partial Z} \right) \mathrm{d}\Omega = \widehat{A_Z} S_T$$

$$\iint_T \left(\frac{\partial F_y}{\partial Z} + S_y \frac{\partial U}{\partial Z} \right) \mathrm{d}\Omega = \widehat{B_Z} S_T \tag{37}$$

In the preceding equation $\partial U/\partial Z$ describes a similarity transformation between ∂U and ∂Z. It is quite difficult to determine $\bar{Z}$ from Eq. (37) because the MHD flux (3) is a highly nonlinear function of the conservative state vector and in general of any parameter vector Z.

In the pure hydrodynamical case the choice of Roe's parameter vector $Z = \sqrt{(\rho)}[1, u, v, w, (E + p)/\rho]^T$ significantly simplifies the problem because the source term vanishes and the flux vector can be written as a quadratic function of the Roe variables. This choice results in Jacobian matrices $\widehat{A_Z}$ and $\widehat{B_Z}$, which are linear in Z. These can be integrated exactly by computing the arithmetic average of the Roe variables at the vertices of a triangle and using these averages in the analytic expression of the Jacobians. The main difficulty in the solution of the MHD equations by the fluctuation splitting method is that such a parameter vector does not exist, which yields merely second-order fluxes, as a result of additional terms proportional to the magnetic field. Although a Roe parameter vector is defined for the MHD equations,[14] it results in a highly nonlinear flux function precluding the simple extension of the multidimensional Roe linearization for MHD flows.

Instead of aiming at a complete exact linearization for the MHD equations, we use a more pragmatic approach, which yields exact conservation of most terms in the fluxes and exact integration of all but one component of the source term under the assumption of linear variation of a certain parameter vector. The source term in the energy equation is approximately integrated. The remaining error in the conservation of the convective fluxes is easily evaluated and distributed to the nodes of the triangle by a nonmonotone scheme. Theoretically the schemes can loose their positivity because of this correction for conservation, but in practice they produce an oscillation-free solution across discontinuities.

Let us consider the following parameter vector W:

$$W = (\rho, u, v, w, B_x, B_y, B_z, H)^T \tag{38}$$

where H is the total enthalpy defined by

$$H = \gamma/(\gamma-1)p + \tfrac{1}{2}\rho \boldsymbol{v}\cdot\boldsymbol{v} + \boldsymbol{B}\cdot\boldsymbol{B} \tag{39}$$

One easily verifies that the MHD flux vector $\boldsymbol{F}$ is at most cubic in terms of W. More specifically, the mass flux and the flux of the induction equation contain only quadratic terms. The momentum flux is built up from linear, quadratic, and some cubic terms, and the energy flux contains quadratic and cubic terms. Let us write $\boldsymbol{F}$ in the following form:

$$\boldsymbol{F} = \boldsymbol{F}^{(2)} + \boldsymbol{F}^{(3)} \tag{40}$$

where $\boldsymbol{F}^{(3)}$ contains the third order and $\boldsymbol{F}^{(2)}$ contains the linear and quadratic components of the MHD flux function, in terms of W. Assuming linear variation of W, we can easily compute the average of the state vector $\bar{W}$ over a triangle:

$$\bar{W} = \frac{1}{S_T}\iint_T W \,\mathrm{d}\Omega = \frac{1}{3}\sum_{i=1}^{3} W_i \tag{41}$$

Using state $\bar{W}$ in the Jacobians corresponding to the flux term $\boldsymbol{F}^{(2)}$ results in an exact conservation of these fluxes. However, the Jacobians corresponding to $\boldsymbol{F}^{(3)}$ are second order in W; therefore, we make an error in the conservation of these fluxes and in the satisfaction of Eq. (36) if we base our scheme on the linearized state $\bar{W}$.

To compensate for this error, we introduce a correction step into our distribution scheme. This step can be done at the same time as the usual distribution; therefore, it is not needed to construct a real two-step method.

In practical computations first we base the whole distribution scheme on the linearized state $\bar{W}$ just described. This choice leads to the following nonconservative total residual $\Phi^{(3)}_{\mathrm{NC}}$ (based on the quasilinear form) corresponding to the cubic fluxes:

$$\Phi^{(3)}_{\mathrm{NC}} = S_T\left[\left(\frac{\partial F^{(3)}_x}{\partial W}\right)_{\bar{W}} + \left(\frac{\partial F^{(3)}_y}{\partial W}\right)_{\bar{W}}\right]\cdot\nabla W \tag{42}$$

The conservative residual $\Phi^{(3)}_C$ of the cubic fluxes can be exactly computed as

$$\Phi^{(3)}_C = \oint_{\partial V} \boldsymbol{F}^{(3)}(W)\cdot\boldsymbol{n}\,\mathrm{d}S \tag{43}$$

assuming linear variation of the parameter vector W. The conservation error of the convective fluxes in conservative variables is

$$\delta\Phi = \Phi^{(3)}_C - \Phi^{(3)}_{\mathrm{NC}} \tag{44}$$

The correction $\delta\Phi$ is distributed to the nodes either by using simple central Galerkin distribution or by any of the linearity preserving schemes. In this paper we use the LDA distribution scheme for distributing the correction of the fluctuation. The distributed residual Φ^T_i in a triangle to node i can be written in the following compact way:

$$\Phi^T_i = \Phi^S_i + \beta^{\mathrm{LDA}}_i \delta\Phi \tag{45}$$

where Φ^S_i is computed by using the selected monotone distribution scheme (FV, N, B schemes, the main part of the distribution) and β^{LDA}_i is the distribution matrix of the LDA scheme.

As just discussed, because of the particular choice of W several terms in the correction $\delta\Phi$ vanish. Nonvanishing terms correspond to part of the momentum and energy fluxes. This implies for the MHD equations that W contains the components of the magnetic field themselves.

It is clear that the quality of the solution of a given problem will be mainly determined by the chosen distribution scheme, whereas the linearity preserving nonmonotone LDA scheme used for the distribution of the correction produces only a minor contribution. However, theoretically the monotonicity property of the positive distribution schemes cannot be guaranteed anymore by our method. Practical computations have revealed that discontinuities are captured without spurious oscillations typical to second-order nonpositive schemes. Even distributing the conservation error $\delta\Phi$ by a simple central Galerkin distribution did not show significant differences.

Because the generalized upwind parameters K^+_i and K^-_i are defined through the partial derivatives of the flux function with respect to the conservative variables, the consistent gradient of the conservative variables U is introduced by

$$\widehat{\nabla U} = \frac{\partial U}{\partial W}(\bar{W})\nabla W \tag{46}$$

This definition leads to the following integral form of the quasi-conservative equation (6):

$$\iint_T \frac{\partial U}{\partial t}\,\mathrm{d}\Omega + S_T\left[A_U(\bar{W})\frac{\widehat{\partial U}}{\partial x} + B_U(\bar{W})\frac{\widehat{\partial U}}{\partial y}\right] = 0 \tag{47}$$

which is equal to the integral form of Eq. (10) with constant Jacobians per cell and with the assumption that W varies linearly.

The presented approximate linearization with the correction technique to ensure the conservation of the convective fluxes can be applied for any other hyperbolic systems, where the Roe linearization fails to yield exact conservation as a result of the higher-order fluxes or when the Roe average is not appropriate for other reasons.

Another solution for the linearization of nonlinear hyperbolic systems admitting an entropy inequality is proposed in a recent work of Abgrall and Barth.[25] They present a nonconservative linearization combined with an adaptive quadrature and demonstrate that the scheme conveys to the weak solution if the precision of the quadrature is increased for large cell residuals. This method can also be used in the context of the MHD equations, and it will be considered in a subsequent work of the authors of this paper.

Notes on the Nonconservative Nature of the Eight-Wave Model

For the set of ideal MHD equations, a second problem appears concerning the conservation of the convective fluxes, namely the presence of Powell's source term, which cannot be written in a divergence form. As noted before, inclusion of Powell's source term into the formulation of the governing equations is essential for the regularity of the Jacobians needed in the fluctuation splitting approach. However, its nonconservative nature can lead to inconsistent jumps accross discontinuities. Indeed, in a recent paper of Toth[16] the author presents a test problem, which clearly shows that the eight-wave equations converge to wrong jumps accross the fast shocks present it that specific problem. Although this test case appropriately demonstrates this weak point of the eight-wave equations, one should not draw final conclusions concerning their applicability. The eight-wave formulation has been succesfully used since its appearance in many astrophysical computations, and several numerical tests were done to check the convergence of the solution in the presence of discontinuities with positive results.[15,17,26]

Numerical experiments indicate that the error caused by the source term mainly depends on three conditions. These are the physical problems in hand; the geometry of the grid compared to the orientation of the discontinuities in the problem and of course the applied numerical scheme. In the absence of a convincing theoretical study, an extensive parametric investigation could be done to yield a guide, showing under which cirumstances the eight-wave model can be used without the presence of significant disturbing errors caused by the source term. The simulation results in the references just given indicate that the eight-wave model works well for a large variety of steady shocks on the considered meshes.

As an example for the computation of proper jump relations on a set of refined grids, we present numerical test in the next part of this paper concerning the problem of a superfast magnetized flow over a perfectly conducting wedge containing a fast shock.

Time-Integration Methods

To integrate Eq. (10) in time, we use explicit and implicit time-marching procedures. The explicit schemes are robust and straightforward to implement, but the time step is limited because of stability

considerations. The limited time step slows down the convergence towards the steady state.

Implicit schemes show better stability properties, allowing much larger time steps and faster convergence, but they require the construction and solution of large linear systems at every time step, making the implementation more complicated.

Explicit Forward Euler Scheme

For the explicit time integration we use the simple forward Euler method. Discretization of Eq. (24) in time leads to the following form:

$$U_i^{n+1} = U_i^n - \frac{\Delta t_i}{S_i} \sum_{T,\, i \in T} \beta_i^T \Phi^T \tag{48}$$

The time step Δt_i is limited because of consideration of stability. To speed up the convergence toward the steady state, local time stepping is used, which means that Δt_i is computed locally, for every node. This destroys the first-order time accuracy, but it does not influence the spatial accuracy of the solution at the steady state.

Implicit Backward Euler Scheme

To perform implicit solution of Eq. (10), we extend implicit integration strategies for solving compressible flow equations.[27] Here we just give a short summary of the method; the reader is referred to the preceding reference for more details.

The evaluation of the residual $R(U)$ at time level $n+1$ results into the following implicit temporal discretization:

$$\frac{U^{n+1} - U^n}{\Delta t} = R(U^{n+1}) \tag{49}$$

Equation (49) consists of a set of nonlinear algebraic equations for the nodal state vectors U^{n+1}, which is solved in an iterative way by Newton's method. Because we are only interested in the steady-state solution of Eq. (10), it is enough to solve Eq. (49) approximately by performing only the first step of the Newton iteration, thus obtaining the linear backward Euler method:

$$\left[\frac{I}{\Delta t} - \frac{\partial R}{\partial U}(U^n)\right](U^{n+1} - U^n) = R(U^n) \tag{50}$$

Equation (50) is a linear system of equations for U^{n+1}, which is again solved approximately. The Jacobian matrix $\partial R/\partial U(U^n)$ is computed numerically by using a first-order numerical approximation. The linear system (50) is transformed into a better conditioned system by using the incomplete upper–lower (ILU) preconditioner, and the resulting system of equations is solved by a Krylov subspace method such as the generalized minimum residual (GMRES) method.

MHD Flow Solver

The fluctuation splitting spatial discretization technique combined with the time-integration strategies are used in order to set up an upwind multidimensional ideal MHD code on unstructured grids composed of triangles. This code advances the solution toward the steady state by a time marching procedure starting from a uniform initial state.

To fully determine the problem, we prescribe boundary conditions at the boundaries of the computational domain. Technically these boundary conditions are imposed in a weak manner, meaning that the inner numerical scheme is used at the boundary on degenerated triangles, called *ghost cells*.

The divergence-free condition of the magnetic field is enforced weakly by using Powell's source term. For explicit and for implicit computations we use the simple forward Euler and backward Euler schemes, respectively. The convergence of the solution is monitored by the L_2 norm of the density residual $||\Phi^\rho||_2$

$$\|\Phi^\rho\|_2 = \sqrt{\frac{1}{N}\sum_{i=1}^{N}\left(\Phi_i^\rho\right)^2} \tag{51}$$

where N is the number of nodes in the computational domain. The stopping criterium for the state of convergence is

$$\log_{10}\|\Phi^\rho\|_2 < -15 \tag{52}$$

Simulation Results

Accuracy of the Schemes: Expanding Flow over a Bend

To determine the numerical accuracy of the fluctuation splitting schemes presented in this paper, first a grid-convergence study on regular unstructured meshes is performed. The steady MHD flowfield for a supermagnetosonic expansion over a convex wall is computed for four different cell sizes for all of the presented residual distribution schemes (FV, N, LDA, B). The average size of the cells in decreasing order is $h_1 = 20^{-1}$, $h_2 = 40^{-1}$, $h_3 = 60^{-1}$, $h_4 = 80^{-1}$.

The flow enters the domain from the left with a uniform speed faster than the fastest magnetosonic (supermagnetosonic) speed. After a short straight part the plasma starts to expand over the lower wall of the tube, and it leaves at the right with a supermagnetosonic speed. In this case the flow speed remains supermagnetosonic in the whole computational domain. The top and the bottom boundaries are set up as ideal perfectly conducting walls. In the initially imposed uniform flowfield the density $\rho = 1$, the velocity vector $\boldsymbol{v} = (6, 0, 0)$, the magnetic vector $\boldsymbol{B} = (2, 0, 0)$, and the thermal pressure $p = 1$.

In smooth, ideal, steady, magnetic field-aligned flow with uniform supermagnetosonic inlet boundary the stagnation enthalpy H_s, the entropy s, and the quantity ρ/α are constant in the whole simulation domain[3]:

$$H_s = \gamma/(\gamma - 1)(p/\rho) + \tfrac{1}{2}(u^2 + v^2 + w^2) \tag{53}$$

$$s = p/\rho^\gamma \tag{54}$$

$$\rho/\alpha = \rho(|v|/|\boldsymbol{B}|) \tag{55}$$

By computing the mean norm of these quantities on grids with different sizes, we can estimate the accuracy of the numerical schemes.[7] Table 1 shows the computed orders for the FV, N, LDA, and B schemes.

All of the linear schemes converged up to machine accuracy according to convergence indicator (52). However, the nonlinear blended scheme converged approximately 4–5 orders of magnitude, and the convergence indicator stagnated by producing some small amplitude noise.

Theoretical prediction of the formal accuracy of the residual distribution schemes based on a Petrov–Galerkin finite element interpretation of the schemes reveals that the linearity preserving schemes are expected to have an accuracy at least order of 1.5 on arbitrary meshes.[7] Full second-order accuracy can be achieved for certain fully uniform triangulations. However, in practice we refer to these schemes as *second-order-accurate schemes* by keeping in mind that actually they can be slightly less accurate. Similarly, analysis of the linear positive schemes predicts an accuracy at least of order 0.5 for arbitrary distorted meshes. These schemes are referred to as *first-order schemes*.

The numerical results (Table 1) verify the theoretical predictions, and they are in harmony with the conclusions of Paillère.[7] The FV scheme on the median dual cell and the N scheme produce practically first-order results. Both of these schemes are linear and positive. The nonmonotone linear LDA scheme and the monotone nonlinear B scheme show second-order accuracy according to the expectations.

Time-Stepping Strategies: Superfast Nozzle Flow

To demonstrate the performance of the implemented implicit solution strategies, we compute the steady flowfield in a magnetic nozzle both with explicit and implicit methods, and we compare

Table 1 Measured convergence rate of several distribution schemes on the smooth expanding flow test case

Scheme	H_s	s	ρ/α
FV	0.65	0.81	0.48
N	0.87	0.88	0.36
LDA	1.79	1.91	1.83
B	1.76	1.77	1.65

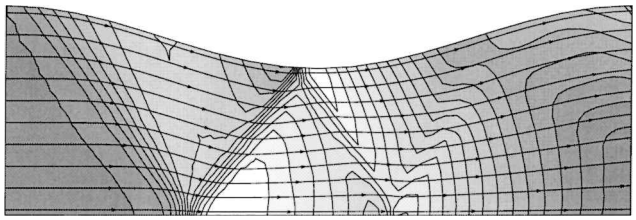

Fig. 2 Shaded density isolines superimposed by magnetic field lines for the magnetic nozzle test case: implicit result.

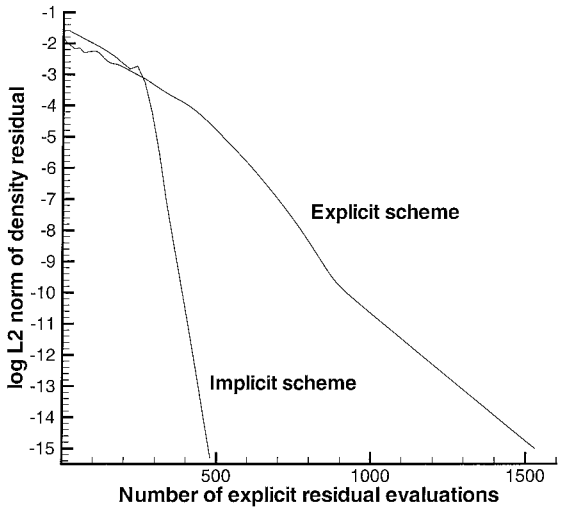

Fig. 3 Convergence histories for the magnetic nozzle test case. Explicit and implicit results are indicated.

the performances. The supermagnetosonic flow enters the nozzle from the left (Fig. 2) and leaves it at the right with a supermagnetosonic speed. At the bottom and at the top of the nozzle, we impose symmetric and ideal perfectly conducting wall boundary conditions, respectively. In the initially imposed uniform flowfield the density $\rho = 1$, the velocity vector $\boldsymbol{v} = (3, 0, 0)$, the magnetic vector $\boldsymbol{B} = (2, 0, 0)$, and the thermal pressure of the plasma $p = 0.6$. We use the first-order linear system N scheme for the distribution scheme. In the explicit computations the Courant–Friedrichs–Lewy (CFL) number is $\mathrm{CFL}_{\mathrm{exp}} = 0.9$. In the implicit computations the starting CFL number is $\mathrm{CFL}_{\mathrm{start}} = 0.5$, and the maximum CFL number is $\mathrm{CFL}_{\mathrm{max}} = 1000$. The number of nodes in the unstructured grid is 1035.

The resulting flowfield is shown in Fig. 2. The magnetic field lines are superposed on the shaded density contour plot. Comparison of the explicit and the implicit results on the same mesh shows that the two methods converged to the same steady state up to machine accuracy.

In Fig. 3 we compare the convergence history both for the explicit and for the implicit computations. The L_2 norm of the density residual is plotted as a function of the number of explicit residual evaluations. One implicit time step requires 24 explicit residual evaluations, in order to compute the numerical Jacobian. The gain factor in CPU time in this particular test case was 2.1 in favor of the implicit scheme. It is known that the explicit schemes have the best performance in case of high-Mach-number flows, and the gain factor in CPU time is much higher in favor of the implicit schemes for low-Mach-number simulations.

Shock-Capturing Property: Flow over a Wedge

It was pointed out that Powell's source term is an essential element of our formulation. In principle the presence of this nonconservative source term can disturb the shock-capturing properties of any scheme. However, experience by many authors[15,17,26] has shown that in several cases the nonconservative error caused by the source term is much smaller than other errors appearing because of the numerical discretization. In these cases even convergence of the numerical solution toward the exact solution can be shown for reasonably fine meshes. This is numerically verified for the computation of an oblique shock with known exact solution.

The supermagnetosonic-field-aligned MHD flow enters the domain at the left, falls onto a wedge with straight boundaries, and leaves at the right with a supermagnetosonic speed. The top and the bottom walls are ideal, perfectly conducting walls. For known inflow values and wedge angle it is possible to determine the analytical solution of this test problem. At the uniform inlet the plasma density $\rho = 1$, the velocity vector $\boldsymbol{v} = (6, 0, 0)$, the magnetic field vector $\boldsymbol{B} = (2, 0, 0)$, and the thermal pressure $p = 1$. The angle of the wedge $\alpha = 20$ deg. It is easy to verify that the solution of this configuration is a straight fast shock penetrating from the singular point of the wedge. The downstream state can be determined from the Rankine–Hugoniot jump relations, giving for the plasma density $\rho = 1.9736$, the velocity vector $\boldsymbol{v} = (5.1687, 1.8813, 0)$, the magnetic vector $\boldsymbol{B} = (3.4003, 1.2376, 0)$, and the thermal pressure $p = 4.2413$.

The steady flowfield is computed for all of the fluctuation splitting schemes on a sequence of subsequently refined grid, and the accuracy of the state variables for the whole domain is checked, based on the grid-convergence study briefly discussed in the preceding subsection. We found that for every scheme the discontinuity is captured by jump relations with an order of accuracy of 0.5–0.9, depending on the numerical scheme and on the variable itself.

On the figures we show the second coarsest grid of our sequence (Fig. 4) and the corresponding solutions for the N (Fig. 5), LDA (Fig. 6), and B (Fig. 7) scheme. The N scheme smoothly captures

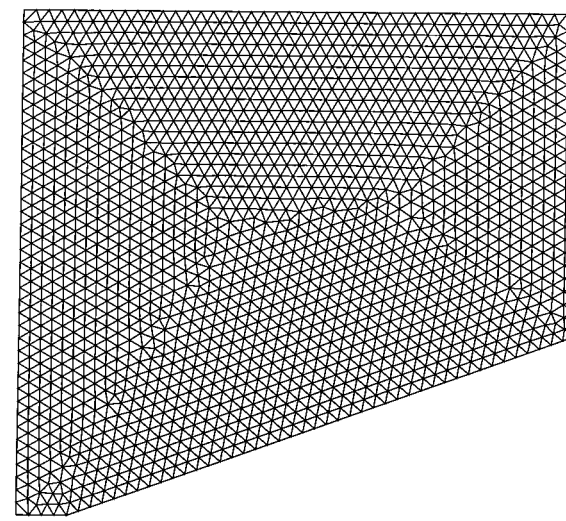

Fig. 4 Unstructured grid for oblique shock over a wedge (1763 nodes).

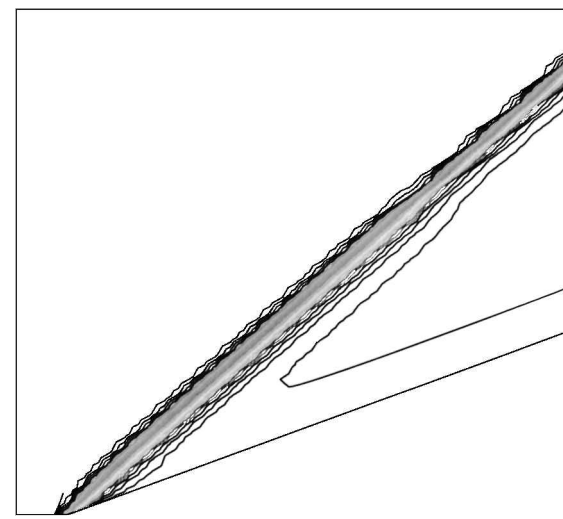

Fig. 5 Density isolines for the oblique shock test case: N scheme.

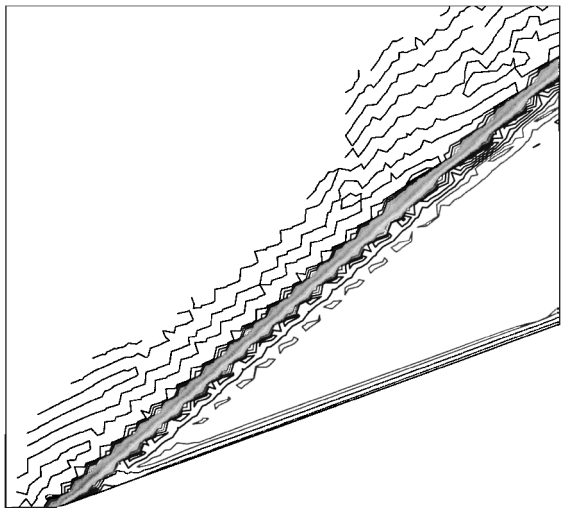

Fig. 6 Density isolines for the oblique shock test case: LDA scheme.

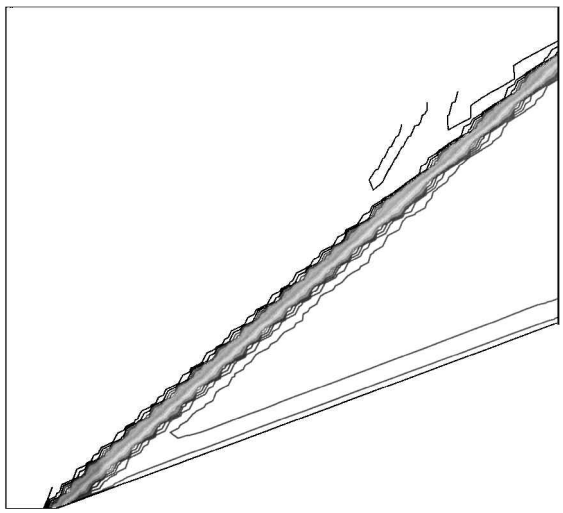

Fig. 7 Density isolines for the oblique shock test case: B scheme.

the discontinuity, but the shock width is diffused because of its first-order accuracy. The LDA scheme produces oscillations in the upstream domain because it is second-order accurate and linear. The B scheme yields the best solution with its oscillation-free sharp shock transition.

Multidimensional Upwinding: Superfast Nozzle Flow

A definite advantage of the fluctuation splitting approach compared to standard finite volume schemes is the compactness of the stencil. The stencil only includes the surrounding nodes around a certain node, even for the second-order schemes. This enables a very efficient coding and lower storage for the implicit matrix. Another advantage compared to dimensionally split schemes is that the presented fluctuation splitting schemes use true multidimensional upwind information. This results in a much sharper shock-capturing property and higher accuracy. The presentation of a full comparison of the residual distribution and finite volume schemes would require an extensive detailed study, which is beyond the scope of this paper. Here we demonstrate the consequence of the true multidimensional upwind property on a single example repeating the supermagnetosonic nozzle flow test case described earlier.

In this test case we choose the fluctuation splitting first-order N and the second-order B scheme on unstructured grids. Concerning the finite volume computation, we use a different code operating on structured cell centered quadrilaterals. The code consists of a dimensionally split Roe-type approximate Riemann solver.[14] Second-order spatial accuracy is achieved via MUSCL reconstruction of the primitive variables at the interfaces, employing the minmod, van Leer, or Van Albada limiter. Temporal integration is done by a multistage Runge–Kutta method. Because of their construction, the residual distribution schemes for the MHD equations described in this paper require approximately five times the CPU time needed by the finite volume scheme just discussed to perform a given number of explicit time steps.

The number of nodes in the unstructured mesh used for the fluctuation splitting scheme is 2662, and the number of volumes for the structured mesh used for the finite volume computation is 2700.

Figures 8 and 9 show the unstructured and structured grids, respectively. The solution of the N, B, and the Roe-type finite volume scheme is given on Figs. 10–12, respectively. Comparison between the minmod and van Albada limiter showed no significant difference

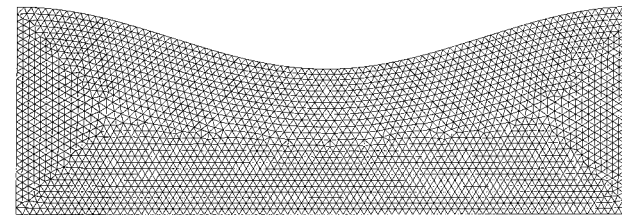

Fig. 8 Magnetic nozzle flow. Unstructured triangulation for the fluctuation splitting code (2662 nodes).

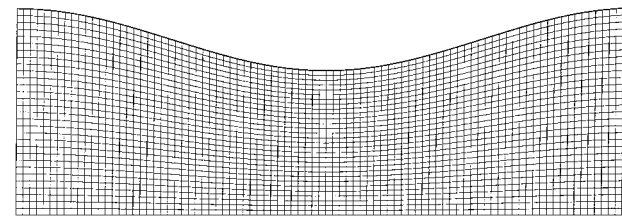

Fig. 9 Magnetic nozzle flow. Structured quadrilaterals for the Roe-type scheme in the finite volume code (2700 cells).

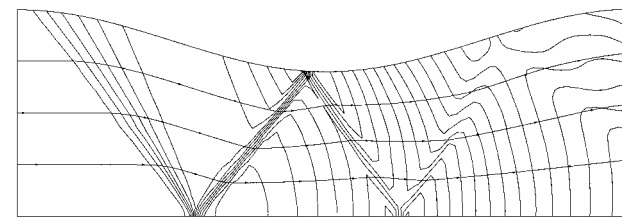

Fig. 10 Density isolines superimposed by magnetic field lines for the magnetic nozzle test case: N scheme.

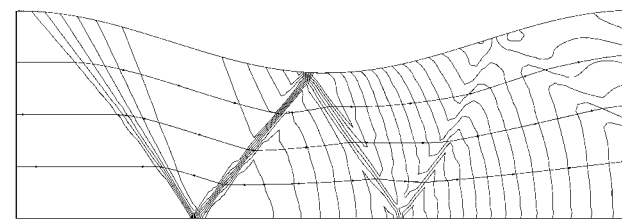

Fig. 11 Density isolines superimposed by magnetic field lines for the magnetic nozzle test case: B scheme.

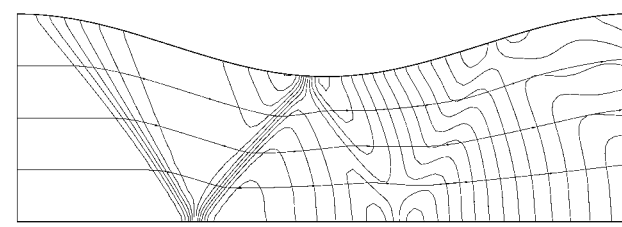

Fig. 12 Density isolines superimposed by magnetic field lines for the magnetic nozzle test case: Roe-type finite volume scheme.

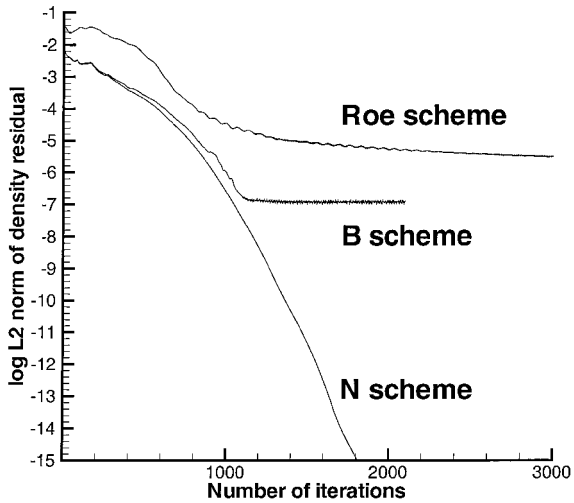

Fig. 13 Convergence history for the magnetic nozzle test case computed by the fluctuation splitting N and B scheme and by a standard Roe-type dimensionally split finite volume scheme.

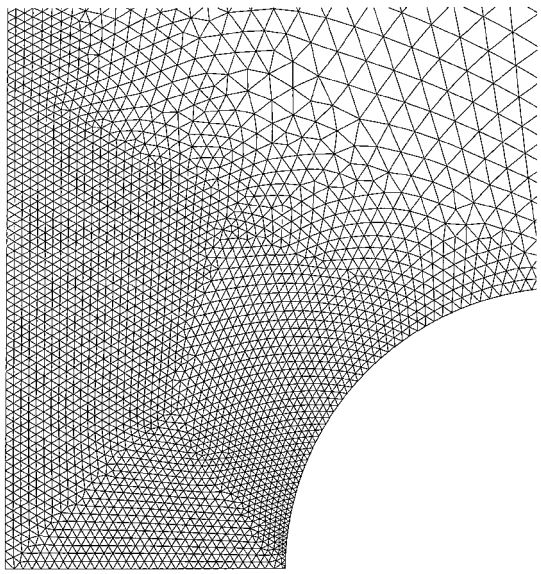

Fig. 14 Part of the unstructured grid used for the magnetic bow shock computation.

for this test case. The results demonstrate that the computation done on a structured mesh with a standard finite volume code produces the most diffusive shock structure, even more diffusive than the first-order fluctuation splitting N scheme. The fluctuation splitting B scheme captures the first reflected shock within two triangles. The last reflected shock is hardly visible on the result of the finite volume code, and it is still pronounced on both fluctuation splitting results.

In Fig. 13 we present the convergence history of these computations. The first-order N scheme converged up to machine accuracy, the B scheme converged five orders of magnitude, and the Roe-type finite volume scheme converged four orders of magnitude.

Bow Shock over a Cylinder

We perform the numerical simulation of an ideal magnetic field aligned flow over a perfectly conducting cylinder. This test case has a very easy setup and serves as a basis of many space physics applications, like bow shock over planets and comets in the solar wind or bow shocks driven by coronal mass ejections. Initially we impose a uniform flowfield on the computational domain, and we use a time-marching procedure toward the steady state. The flow enters the domain at the left with a supermagnetosonic speed, turns around the cylinder, and leaves at the right with a supermagnetosonic speed. The center of the cylinder is situated at $x = 0$, $y = 0$, and its radius is $r = 0.125$.

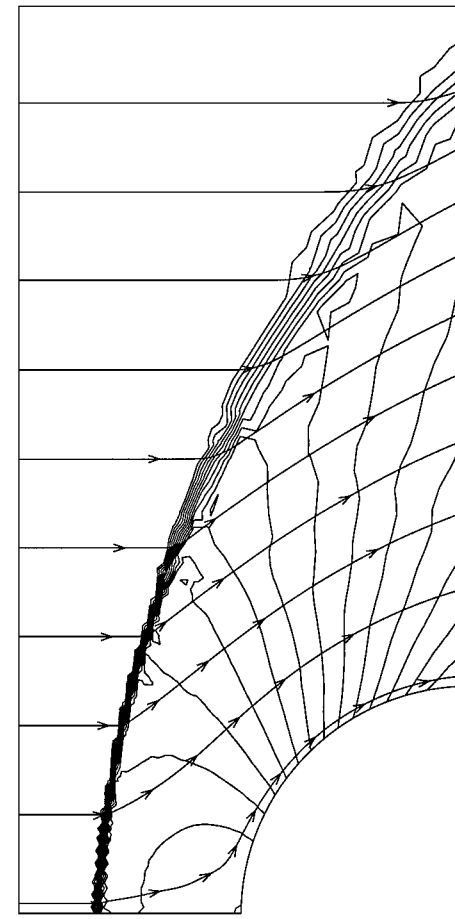

Fig. 15 Magnetic bow shock. Total pressure isolines superimposed by the magnetic field lines (3203 nodes).

Because of symmetry reasons, we compute the flowfield over the left upper quadrant of the cylinder, and the solution is symmetric with respect to the x axes. Part of the unstructured grid is shown on Fig. 14. The symmetry line and the cylinder satisfy perfectly conducting ideal wall boundary conditions, and we prescribe supermagnetosonic outlet at the right. In the initially imposed uniform flowfield the density $\rho = 1$, the velocity vector $\boldsymbol{v} = (3, 0, 0)$, the magnetic vector $\boldsymbol{B} = (1, 0, 0)$, and the thermal pressure of the plasma $p = 0.2$.

Figure 15 shows a global view of the resulting flowfield computed by the nonlinear second-order B scheme. The total pressure isolines are superimposed by the magnetic field lines. This test case converged two orders of magnitude only, and the convergence indicator stagnated. This seems to be the result of the conservative correction, which is sensitive to the present strong normal shock. By switching off the conservative correction, we can achieve much better convergence of the B scheme for this particular test case without changing visibly the solution.

Conclusions

Monotone multidimensional upwind residual distribution schemes have been extended to the solution of the ideal MHD equations. The new schemes have advantages compared to standard finite volume schemes in terms of the compactness of the stencil and accuracy. An approximate conservative linearization technique was developed for general hyperbolic systems together with a conservative correction. Both explicit and implicit time-integration strategies were briefly discussed. The properties of the schemes were demonstrated numerically. Test results revealed that the shock-capturing property of the schemes are not disturbed by the inclusion of Powell's source in the particular test computation. Simulation of supermagnetosonic flow in a magnetic nozzle with several shock reflections gave a numerical example that our multidimensional schemes yield sharper shocks than basic dimensionally split finite volume techniques. We

also presented simulation results of a Mach 3 magnetic-field-aligned MHD flow over a perfectly conducting cylinder. Our main goals in the future are to improve our implicit techniques, to parallelize the code, to extend the schemes to three spatial dimensions, and to include nonideal MHD effects.

Acknowledgment

This research was founded by the Fonds voor Wetenschappelijk Onderzoek (F.W.O. Project G0344.98).

References

[1]Poedts, S., Kerner, W., Goedbloed, J. P., Keegan, B., Huysmans, G. T. A., and Schwarz, E., "Damping of Global Alfvén Waves in Tokamaks due to Resonant Absorption," *Plasma Physics Controlled Fusion*, Vol. 34, No. 8, 1992, pp. 1397–1422.

[2]Priest, E. R., "Solar Magnetohydrodynamics," *Geophysics and Astrophysics Monographs*, edited by B. M. McCormac, D. Reidel, 1982.

[3]De Sterck, H., Low, B. C., and Poedts, S., "Characteristic Analysis of a Complex Two-Dimensional Magnetohydrodynamic Bow Shock Flow with Steady Compound Shocks," *Physics of Plasmas*, Vol. 6, No. 3, 1999, pp. 954–968.

[4]Roe, P. L., "Fluctuations and Signals—A Framework for Numerical Evolution Problems," *Numerical Methods for Fluid Dynamics*, Academic Press, New York, 1982, pp. 219–257.

[5]Deconinck, H., Roe, P., and Struijs, R., "A Multidimensional Generalization of Roe's Flux Difference Splitter for the Euler Equations," *Journal of Computers and Fluids*, Vol. 22, No. 3, 1993, pp. 215–222.

[6]Paillére, H., Deconinck, H., and Roe, P. L., "Conservative Upwind Residual Distribution Schemes Based on the Steady Characteristics of the Euler Equations," AIAA Paper 95-1700, June 1995.

[7]Paillère, H., "Multidimensional Upwind Residual Distribution Schemes for the Euler and Navier-Stokes Equations on Unstructured Grids," Ph.D. Dissertation, Dept. of Fluid Mechanics, Univ. Libre de Bruxelles, Brussels, Belgium, June 1995.

[8]Deconinck, H., Struijs, R., and Roe, P. L., "Fluctuation Splitting for Multidimensional Convection Problems: an Alternative to Finite Volume and Finite Element Methods," von Karman Inst., VKI LS 1990-03, Sint-Genesius-Rode, Belgium, March 1990.

[9]Struijs, R., Deconinck, H., and Roe, P. L., "Fluctuation Splitting Schemes for the 2D Euler Equations," von Karman Inst., VKI LS 1991-01, Sint-Genesius-Rode, Belgium, Feb. 1991.

[10]van der Weide, E., and Deconinck, H., "Positive Matrix Distribution Schemes for Hyperbolic Systems, with Application to the Euler Equations," *Proceedings of the 3rd ECOMAS Computational Fluid Dynamics Conference*, edited by J.-A. Désidéri, C. Hirsch, P. Le Tallec, M. Pandolfi, and J. Périaux, Wiley, Chichester, England, U.K., 1996, pp. 747–753.

[11]van der Weide, E., Deconinck, H., Issman, E., and Degrez, G., "Parallel, Implicit, Multi-Dimensional Upwind, Residual Distribution Method for the Navier–Stokes Equations on Unstructured Grids," *Computational Mechanics*, Vol. 23, No. 2, 1999, pp. 199–208.

[12]Jameson, A., "Artifical Diffusion, Upwind Biasing, Limiters and Their Effect on Accuracy and Multigrid Convergence in Transonic and Hypersonic Flows," AIAA Paper 93-3359, June 1993.

[13]Godunov, S. K., "Symmetric Form of the Equations of Magnetohydrodynamics," *Numerical Methods for Mechanics of Continuum Medium*, Vol. 1, 1972, pp. 26–32.

[14]Powell, K. G., Roe, P. L., Myong, R. S., Gombosi, T. I., and De Zeeuw, D. L., "An Upwind Scheme for Magnetohydrodynamics," AIAA Paper 95-1704, June 1995.

[15]Powell, K. G., Roe, P. L., Linde, T. J., Gombosi, T. I., and De Zeeuw, D. L., "A Solution-Adaptive Upwind Scheme for Ideal Magnetohydrodynamics," *Journal of Computational Physics*, Vol. 154, No. 2, 1999, pp. 284–309.

[16]Toth, G., "The $\nabla \cdot B = 0$, Constraint in Shock-Capturing Magnetohydrodynamics Codes," *Journal of Computational Physics*, Vol. 161, No. 2, 2000, pp. 605–652.

[17]De Sterck, H., Csík, Á., Vanden Abeele, D., Poedts, S., and Deconinck, H., "Stationary Two-Dimensional Magnetohydrodynamic Flows with Shocks: Characteristic Analysis and Grid Convergence Study," *Journal of Computational Physics*, Vol. 166, No. 1, 2001, p. 28.

[18]Jackson, J. D., *Classical Electrodynamics*, Wiley, New York, 1962, p. 315.

[19]Brio, M., and Wu, C. C., "An Upwind Differencing Scheme for the Equations of Ideal Magnetohydrodynamics," *Journal of Computational Physics*, Vol. 75, No. 2, 1988, pp. 400–422.

[20]Roe, P. L., and Balsara, D. L., "Notes on the Eigensystem of Magnetohydrodynamics," *SIAM Journal of Applied Mathematics*, Vol. 56, No. 1, 1996, pp. 57–67.

[21]Barth, T. J., "An Introduction to Recent Developments in Theory and Numerics for Conservation Laws," *Numerical Methods for Gasdynamics Systems on Unstructured Meshes*, edited by D. Kröner, M. Ohlberger, and C. Rohde, Lecture Notes in Computational Science and Engineering, Springer-Verlag, Berlin, 1998, pp. 195–284.

[22]Carette, J. -C., Deconinck, H., Paillere, H., and Roe, P. L., "Multidimensional Upwinding: Its Relation to Finite Elements," *International Journal for Numerical Methods in Fluids*, Vol. 20, No. 8/9, 1995, pp. 935–955.

[23]Deconinck, H., Sermeus, K., and Abgrall, R., "Status of Multidimensional Upwind Residual Distribution Schemes and Applications in Aeronautics," AIAA Paper 2000-2328, 2000.

[24]Abgrall, R., "Toward the Ultimate Conservative Scheme: Following the Quest," *Journal of Computational Physics*, Vol. 167, No. 2, 2001, pp. 277–315.

[25]Abgrall, R., and Barth, T. J., "Residual Distribution Schemes for Conservation Laws via Adaptive Quadrature," *Schémas Distribués en Mécanique des Fluides et Applications,* Écoles CEA-EDF-INRIA, INRIA, 2000, pp. 183–212.

[26]Harada, S., Hoffmann, K. A., and Augustinus, J., "Numerical Solution of the Ideal Magnetohydrodynamic Equations for a Supersonic Channel Flow," *Journal of Thermophysics and Heat Transfer*, Vol. 12, No. 4, 1998, pp. 507–513.

[27]Issman, E., Degrez, G., and Deconinck, H., "Implicit Upwind Residual Distribution Euler/Navier–Stokes Solver on Unstructured Meshes," *AIAA Journal*, Vol. 34, No. 10, 1996, pp. 2021–2028.

K. Kailasanath
Associate Editor